Title
DETERMINATION OF THE ORDERING IN THE INTER-METALLIC COMPOUND Ag2Al BY MEANS OP X-RAYS

Author
Neumann, Joachim P.

Publication Date
1965-01-28

UCRL-11928

University of California

Ernest O. Lawrence Radiation Laboratory

DETERMINATION OF THE ORDERING IN THE INTERMETALLIC COMPOUND Ag_2Al BY MEANS OF X-RAYS

Berkeley, California

DISCLAIMER

UCRL-11928

UNIVERSITY OF CALIFORNIA

Lawrence Radiation Laboratory
Berkeley, California

AEC Contract No. W-7405-eng-48

DETERMINATION OF THE ORDERING IN THE INTERMETALLIC COMPOUND Ag_2Al BY MEANS OF X-RAYS

Joachim P. Neumann

(Ph.D. Thesis)

January 28, 1965

CONTENTS

DETERMINATION OF THE ORDERING IN THE INTERMETALLIC COMPOUND Ag_2Al BY MEANS OF X-RAYS

Joachim P. Neumann

Inorganic Materials Research Division, Lawrence Radiation Laboratory
and Department of Mineral Technology, College of Engineering
University of California, Berkeley, California

January 28, 1965

ABSTRACT

In order to verify the predicted short-range ordering in the intermetallic hexagonal phase Ag_2Al, the diffuse intensity diffracted from single crystals of this alloy was measured in several directions in reciprocal space. On crystals annealed for 10 days at 453°K, the first Cowley-Warren pair-density coefficient was found to be approximately -0.20. The tendency toward the formation of a two-dimensional superlattice on the basal planes is indicated, in which each aluminum atom is surrounded by six silver atoms.

The measurements were carried out in vacuum at approximately 300°K and 150°K, using crystal monochromated Mo K_α-radiation. The proposed model of the superlattice is based on the appearance of short-range order peaks at 1/3 and 2/3 the distance from the (110) line.

Weak but sharp lines of the type (001), (003) can be explained by an average composition difference of 1 at.% in consecutive basal planes, extending over many layers. No explanation can yet be given for the simultaneous existence of long-range and short-range order.

The c-parameter of the annealed alloy was found to be 0.06A larger than the value reported for the quenched alloy, indicating a different atomic arrangement in the two states.

INTRODUCTION

A few years ago Mote, Tanaka and Dorn[1] observed that the critical resolved shear stress for slow prismatic $(10\bar{1}0)\ [1\bar{2}10]$ slip in the hexagonal ζ-phase of an alloy containing 67 atomic percent silver and 33 atomic percent aluminum varied with temperature as shown in Figure 1. Over Region I the yield stress decreased precipitously with an increase in temperature, whereas the yield stress decreased only mildly as the temperature increased over Region II, and again in Region III the yield stress decreased very rapidly with an increase in temperature. In contrast, as shown in Figure 1, the critical resolved shear stress for basal $(0001)\ [1\bar{2}10]$ slip of this alloy, although it exhibited a yield point, was insensitive to the temperature. Detailed investigations by Howard, Barmore, Mote and Dorn[2] have clearly established that prismatic slip over Region III occurs as a result of a diffusion controlled thermally activated dislocation mechanism. Furthermore, Larsen, Rajnak, Hauser, and Dorn[3] have recently in their analyses of the dynamic slip behavior under impulsive loading, attributed the athermal basal slip to Suzuki locking whereas the thermally activated mechanism of prismatic slip that is operative over Region I is controlled by the Peierls' mechanism. Therefore, when the athermal prismatic deformation mechanism that is operative over Region II is determined, complete documentation of the plastic behavior of this particular composition of the ζ-phase in the system silver-aluminum will have been established.

Mote, Tanaka, and Dorn suggested that the high yield stress and the athermal behavior for prismatic slip over Region II could only be ascribed to short-range order hardening. Assuming that the equilibrium degree of short-range order was frozen-in below 475°K, it was possible to solve simultaneously, (a) the conditions for equilibrium giving Cowley's short-range

order parameter in terms of the ordering energy and (b) Fisher's equation of the flow stress as a function of the degree of order and the ordering energy. On this basis the ordering energy was estimated to be more than about -760 cal/mole and Cowley's degree of order for the frozen-in order was not more than about -0.30.

This investigation was undertaken in order to obtain more direct evidence on the possible effect of short-range order on the prismatic slip of the ζ-phase in the system silver-aluminum. Whereas the Ag-rich cubic α-solid solution of Al is known to exhibit short-range ordering[4], and the Al-rich cubic δ-solid solution of Ag is known to exhibit clustering[5], the details concerning the hexagonal ζ-phase are not clear.

Rudman[4] measured the ordering in this phase by means of x-rays at 40 atomic percent aluminum on polycrystalline material quenched from 575°C to room temperature, and estimated that Cowley's degree of order α is about -0.10. He observed however also effects equivalent to differences in atomic radii, which as he himself points out, is unlikely since the lattice parameters of silver and aluminum differ by less than 1% and no size effect is observed in the silver-rich α-solid solution.

It is quite possible that the degree of order in the hexagonal system may be different parallel to and perpendicular to the c-axis. This possibility is emphasized by the concept that whereas prismatic slip in Region II is controlled by short-range order, basal slip over the same temperature range has a lower resolved shear stress and is due to Suzuki locking. Evidently these issues can only be resolved by measuring the diffuse scattering from single crystals of this alloy.

DIFFRACTION THEORY

The intensity of x-rays scattered coherently by crystals containing two types of atoms, A and B, consists of two parts: (Appendix I).

I_F, the intensity of the fundamental reflections, which is independent of the state of order in the crystal and which is concentrated in sharp peaks given by the Bragg relationship:

$$I_F = NI_e(x_A f_A + x_B f_B)^2 \sum_{p=1}^{N} \sum_{q=1}^{N} e^{\frac{2\pi i}{\lambda} \vec{r}_{pq}(\vec{s}-\vec{s}_0)} \qquad (1)$$

I_S, the intensity due to the presence of different kinds of atoms in the crystal, which depends on the distribution of A and B

$$I_S = NI_e x_A x_B (f_A - f_B)^2 \sum_{p=1}^{N} \sum_{q=1}^{N} \left(1 - \frac{p_{AB}(\vec{r}_{pq})}{2x_A x_B}\right) \cdot e^{\frac{2\pi i}{\lambda} \vec{r}_{pq}(\vec{s}-\vec{s}_0)} \qquad (2)$$

with:

- N : the total number of atoms, assumed to be at rest
- I_e : the intensity scattered by one electron
- x_A, x_B : the atomic fractions of A and B
- $\vec{r}_{pq}$: the interatomic vector from the p's atom
- λ : wavelength of the radiation
- $p_{AB}(\vec{r}_{pq})$: the probability of finding an A-B or B-A pair connected by the vector $\vec{r}_{pq}$

In order to get a quantitative measure of the order, Cowley and Warren[6][7] have introduced the short-range order coefficients $\alpha(\vec{r}_{pq})$, defined by:

$$\alpha_{pq} \equiv 1 - \frac{p_{AB}(\vec{r}_{pq})}{2x_A x_B}$$

If no long-range order, but only a finite amount of short-range order exists, the coefficients will approach zero for $\vec{r}_{pq} \to \infty$ since $p_{AB}(\vec{r}_{pq})$ will approach the value of a random solution, $2x_A x_B$. For a perfectly random solution, all $\alpha_{pq} = 0$, except $\alpha_{p=q}$, which will be unity, and Equation (2) yields the Laue monotonic function[8]:

$$I_s = NI_e x_A x_B (f_A - f_B)^2$$

Using the short-range order coefficients α_{pq}, Equation (2) can be rewritten:

$$I_s(eu) = N \cdot I_e \cdot x_A x_B (f_A - f_B) \sum_{p=1}^{N} \sum_{q=1}^{N} \alpha_{pq} e^{\frac{2\pi i}{\lambda} \vec{r}_{pq}(\vec{s}-\vec{s}_0)} \qquad (3)$$

where the total intensity I_s is in terms of the intensity scattered by one electron (in electron units, eu). The intensity in electron units scattered by one atom is:

$$I_s\left(\frac{eu}{atom}\right) = \frac{I_s(eu)}{NI_e}$$

and

$$\frac{I_s\left(\frac{eu}{atom}\right)}{x_A x_B (f_A - f_B)^2} = I'_s = \sum_{p=1}^{N} \sum_{q=1}^{N} \alpha_{pq} e^{\frac{2\pi i}{\lambda} \vec{r}_{pq}(\vec{s}-\vec{s}_0)} \qquad (4)$$

Equation (4) gives the intensity I'_s in form of a Fourier series, with the short range order coefficients being the Fourier coefficients. The coefficients can

be evaluated by harmonic analysis after measuring the intensity as a function of the diffraction vector $(\vec{s} - \vec{s}_0)$. The summation has to be carried out over all distinct interatomic vectors $\vec{r}_{pq}$. No complications from size effect terms should arise[9] in the case under consideration, since the lattice constants of pure aluminum and silver differ by less than 1%.

In a close-packed hexagonal lattice the vector $\vec{r}_{pq} = \vec{r}_q - \vec{r}_p$ from the p's to the q's atom can be described by:

$$\vec{r}_{pq} = \ell \frac{\vec{a}_1}{3} + m \frac{\vec{a}_2}{3} + n \frac{c}{2} \tag{5}$$

where a_1, a_2 and c are the conventional axes and l, m, and n integers with the following restrictions:

n even:	$l = 3g$	
	$m = 3g$	where g = any integer, not necessarily the same
n odd:	$l = 3g \pm 1$	
	$m = 3g \mp 1$	where g = any integer, not necessarily the same

The diffraction vector $(\vec{s} - \vec{s}_0)$ which is perpendicular to the diffracting plane having the intercepts $1/h_1$, $1/h_2$, $1/h_3$ with the crystal lattice axes $a_1/3$, $a_2/3$, $c/2$ can be expressed in terms of the reciprocal lattice axes a_1^*, a_2^*, c^* as: (Appendix II).

$$\frac{\vec{s} - \vec{s}_0}{\lambda} = h_1 a_1^* + h_2 a_2^* + h_3 c^* \tag{6}$$

where:

$$a_1^* = \frac{3}{a_1 \cos^3 0} \qquad c^* = \frac{2}{c}$$

$$a_2^* = \frac{3}{a_2 \cos^3 0}$$

and h_1, h_2, h_3 continuous variables.

Introducing the expressions for $\vec{r}_{pq}$ and $(\vec{s} - \vec{s}_0)$ given by Equations (5) and (6) into Equation (4) one obtains:

$$I'_s = \sum_{\ell}\sum_{m}\sum_{n} a_{Lmn}\, e^{2\pi i(\ell \frac{\vec{a}_1}{3} + m \frac{\vec{a}_2}{3} + n \frac{\vec{c}}{2})\,(h_1 a_1^* + h_2 a_2^* + h_3 c^*)}$$

and

$$I'_s = \sum_{\ell}\sum_{m}\sum_{n} a_{Lmn}\, e^{2\pi i(\ell h_1 + m h_L + n h_3)} \qquad (7)$$

In order to convert the observed intensity from the arbitrary units in which it has been measured (e.g., counts per seconds) into electron units per atom, two methods can be used.

1. One can measure the total intensity in the reciprocal lattice cell, and determine the normalization constant K from the relationship

$$K \sum_{h_1}\sum_{h_2}\sum_{h_3} I'_s = a_{000} \equiv 1$$

This method was used by Cowley[10].

2. One can measure for the same experimental conditions the intensity scattered by a non-crystalline low-atomic number material, whose intensity in electron units per atom (or molecule) can be computed. The normalization constant found in this way is independent of the material and can be used to normalize the intensity of the metallic specimen. This method was used by Norman and Warren[11]. Since in the present investigation only one-dimensional intensity measurements were done, the latter normalization method was employed. The equation for the geometry of a diffractometer, where incident and diffracted beam make the same angle with the specimen surface, is:

$$I(c/|s|) = K \frac{1 + \cos^2 2a \cdot \cos^2 2\theta}{(\frac{\mu}{\rho})\, M} \cdot I\,(\frac{eu}{molecule}) \qquad (8)$$

with:

$(\frac{\mu}{\rho})$: mass absorption coefficient

M : Molecular-unit weight

$2a$: Bragg angle of crystal monochromator

2θ : Diffraction angle of specimen

The polarization correction is for the case where the diffracted beam stays in the same plane. $I(\frac{eu}{molecule})$ consists of coherent and incoherent radiation; its computation for quartz-glass, the standard used in this investigation is given in Appendix III. Appendix V shows the correction to be applied to the mass-absorption coefficient of SiO_2 for MoK_a-radiation because of the wave-length shift of the Compton-radiation. The elimination of extraneous intensity contributions is discussed in the section "Experimental Techniques."

EXPERIMENTAL TECHNIQUES

SPECIMEN PREPARATION

High purity silver and high purity aluminum, both 99.995 wt. % were melted in a zirconium oxide crucible under helium in an induction furnace and cast into a water-cooled copper mold to produce an ingot of 33.2 ±0.3 at. % Al.

Pieces of this ingot were used to grow single crystal spheres of 1 inch diameter, using the modified Bridgman technique with stationary mold and moving furnace. The crystals were grown in graphite molds (spectrographic purity) under vacuum, the furnace velocity was 2.5 cm per hour, the temperature gradient about 15°C/cm.

For the x-ray measurements, flat discs, 0.25 inches thick and 0.75 inches in diameter, are needed. To avoid any mechanical deformation when cutting these discs out of the spheres with the desired orientation, an electric discharge machine was used. The cylindrical surfaces were obtained by means of a tubular brass tool, for the flat surfaces a fork-like tool consisting of two parallel brass sheets were employed. All cutting was done at the lowest spark-energy range. The orientation of the spheres could be easily found by etching them in a solution of 1 vol-part water, 2 vol-parts conc. nitric acid.

After cutting, the crystals were given the following vacuum annealing treatment:

1 day at 650°C, cooled within 5 hours to 180°C, 10 days at (180 ±5°C), air cooled to room temperature.

---

*"Servomet," Metals Research Ltd., Cambridge, England.

Before the final x-ray examination the discs were electrolytically polished in an aqueous solution of 2% potassium cyanide and 2% sodium hydroxide.

MONOCHROMATOR

In order to obtain useful values of the solution-diffuse (Laue-diffuse) scattering, which is of a very low intensity, it is necessary to employ strictly monochromatic radiation obtained by diffraction from a single crystal. In the present investigation Mo K_α-radiation was chosen for the following reasons:

1. The radiation should be absorbed as little as possible in its path, i.e., the wavelength should be short.

2. It should not excite the characteristic radiation of the specimen. Mo K_α (= 0.71 Å) will excite the Ag L_α (L-edge 3.7 Å) but not the Ag K_α radiation (K-edge: 0.49 Å).

3. The intensity measurements should be carried out at low angles, to reduce the effect of temperature[12], i.e., the wavelength should be short.

The monochromator used was a bent $(10\bar{1}1)$ quartz crystal, asymmetrical ground with focal lengths of 80 and 132 mm. It was placed on a water-cooled aluminum arm which was rigidly attached to the x-ray tube. The angular position of the crystal could be adjusted to within 0.003°. The take-off angle was 3°, and the horizontal divergence γ was limited to 0.5°.

The water cooling kept the temperature of the monochromating unit constant to ±1°C.

By adjusting the crystal for maximum α_1-intensity, the α_2-radiation is reduced to 10% of the α_1-radiation, since the optimum θ-settings for the two wavelengths differ by $\Delta\theta = 0.036°$.

From: $\Delta\theta = \frac{\Delta\lambda}{2d}$

with: $\Delta\lambda$ (wavelength difference) = 0.0042 A

d (spacing of $10\bar{1}1$ planes) = 3.34 A

For complete elimination of the α_2-radiation, Frohnmeyer[13] placed a 15 micron wide slit at the focal point, sacrificing thereby also a large fraction of the α_1-radiation. For the present investigation this method would have given too low intensities, and no further reduction of the α_2-radiation was therefore attempted.

A platinum slit, 5 mm high and 115 micron wide, placed at the focal point, let the whole doublet pass and eliminated only stray radiation on either side. Each line had a width of about 70μ, as a result of the apparent width of the line focus of the x-ray tube (40μ) and imperfections of the monochromater crystal.

Preliminary adjustments of the monochrmater were done using a fluorescent screen, the final adjustment by means of photographic plates.

A picture of the monochromating unit, with the tantalum radiation shields removed, is shown in Figure 2.

SPECIMEN-CHAMBER

The diffractometer used for the measurements was a General Electric XRD-5 unit; it was positioned so that the focal point of the monochromator was on the diffractometer circle. The vertical divergence δ of incident and diffracted beam was limited to 2° by means of high-resolution soller-slits. The specimen was mounted at the bottom of a metal Dewar within a vacuum chamber of 10 cm inner diameter. It could be tilted and rotated from the outside about two horizontal axes perpendicular to each other (Figure 3).

The x-rays entered and left through a 0.015 inch beryllium window. The chamber was made of 304 stainless steel except for the bottom of the coolant chamber and the connections to the specimen, which were made of copper. The vacuum served the two-fold purpose of eliminating air-scattering and providing thermal insulation. A flexible metal tubing connected the chamber with the vacuum pumps; a liquid nitrogen trap prevented the back-diffusion of oil-vapors. The temperature was measured with a thermocouple, pressed by a spring against the back of the specimen. The temperature difference between the front and back of the specimen never exceeded 1°C.

By filling the coolant chamber with oil and heating it by means of an immersion heater, it should be possible to use the vacuum chamber if the need arises for investigations up to 300°C.

INTENSITY MEASUREMENTS

The intensities were measured with a scintillation counter No. 3, in connection with a photomultiplier tube with variable voltage, a preamplifier, a linear amplifier with variable gain, and a pulse-height-selector.

A determination of the noise-level as a function of photomultiplier-voltage and linear amplifier-gain showed (Figure 4) that at gain 10 the voltage should not exceed 1150 volts. Since the radiation obtained from the monochromator contains besides the K_α-radiation also its higher-frequency harmonics, if the tube voltage was sufficient to excite them, a pulse height selector can be used to eliminate them.

In order to determine the optimum setting of the discriminator window, "monochromatic" Mo K_α-radiation was diffracted from a lithium-fluoride crystal and the pulse height distributions of the radiations with $\lambda = 0.71$ Å and $\lambda = 0.35$ Å measured, by setting the counter at $2\theta = 20°$ and $2\theta = 10°$, the Bragg-angles corresponding to the (200) reflection of these two wavelengths.

Figure 5 shows for the selected voltage of 1100 volts the position of the two wavelengths. By using a symmetrical window setting from 6.1 to 12.0 volts, the intensity of the half wavelength radiation can be reduced to less than 1%, while the Mo K_α-radiation is still 90% of the value for a window from 4 to 16 volts.

Before being eliminated in the pulse height selector, the half wavelength has however excited the Ag K_α-radiation, which with a wavelength of 0.56 A has its peak at 11.5 volts so that it is only partially eliminated by the pulse-height selector. By varying the window width it was found however that this contribution was negligible.

When using quartz glass for normalization, 60 to 80% of the radiation is incoherent, with a wavelength of:

$\lambda_i = \lambda_c + 0.0242\ (1 - \cos 2\theta)$

For $2\theta = 160°$: $\lambda_i = 0.709 + 0.047 = 0.756$ Å

To insure that the counter has the same efficiency for coherent and incoherent radiation, the window was widened toward the lower voltages to 5.4 volts.

From the relationship V_1 (Volts) x λ_1(Å) = $V_2 \cdot \lambda_2$ it follows that the peak of the incoherent radiation will appear at 8.5 Volts, i.e., 0.5 Volts lower than the peak of the coherent radiation.

In order to prevent radiation scattered by the beryllium window from reaching the counter, the horizontal divergence of the diffracted beam was limited to 3°.

It is not advisable to limit the horizontal divergence of the diffracted beam (γ') to that of the incident beam (γ). For the metal specimen, the diffracting layer can be considered to be infinitely thin, but this is not the case for the standard with its low atomic number. The linear absoprtion coefficient of SiO_2 for Mo K_α-radiation is only 8.0 cm^{-1}, and not all of the diffracted radiation would enter the counter, when using the same divergence for indicent and diffracted beam.

With $\gamma' = 3°$ and $2\theta > 120°$, more than 99.9% of the total diffracted intensity is measured, while still keeping the absorption correction negligible.

The detector slit had a width of 1°. The intensity-measurements were done by step-scanning with fixed-time count (1000 sec), resulting in a standard deviation of 1% or less.

EXTRANEOUS SCATTERING

The total intensity measured by the counter contains beside the Laue-diffuse scattering I_s several extraneous components, which have to be eliminated, before the short-range order coefficients can be evaluated.

1. The background of the counter (Figure 4). It was determined at certain intervals during the measurements of the metal specimen and the standard with the x-ray beam blocked off.

2. The intensity of the fundamental reflection I_F - is eliminated by interpolating the background under the sharp peaks.

3. Air-scattering can be avoided by working in vacuum.

4. Fluorescent radiation from the specimen can be suppressed by proper choice of the incident radiation and by employing a pulse-height selector.

5. Due to the thermal vibrations of the atoms, the intensity of the fundamental reflections is reduced and appears as temperature diffuse scattering I_T in the background, particularly at higher diffraction angles. It can be eliminated by measuring the intensity at a few temperatures below room temperature and extrapolation to 0°K. It is assumed that the short-range order does not change in this temperature region. It has only recently been pointed out[12], that the thermal vibrations will cause a broadening of the short-range-order peaks in the same way they influence the fundamental peaks. This error has not been considered in previous determinations of the short-range-order; it can be reduced by use of a short-wavelength radiation.

6. After contributions 1 to 5 have been subtracted, the remaining intensity has to be put into electron units per atom, before the last extraneous scattering can be eliminated, the incoherent scattering I_i from the specimen. It has been measured or computed in electron units per atom as shown in Appendix VI for both aluminum and silver.

Since the incoherent scattering from the silver-aluminum specimen accounts for only a few percent of the coherent diffuse scattering, and since at low angles the wavelength shift is small, the mass absorption coefficient for the coherent Mo K_α-radiation was taken without correction[14].

$$\left(\frac{\mu}{\rho}\right)_{Ag_2Al} = 23.5 \frac{cm^2}{g}$$

$$M_{Ag_2Al} = 242.7$$

The atomic scattering factors of silver and aluminum, as taken from the International Tables and corrected for Mo K_α-radiation, are given in Appendix VII.

EXPERIMENTAL RESULTS

A. Intensity Measurements of SiO_2-Standard

In order to determine the normalization constant K in the equation:

$$K = \frac{(\mu/\rho)\, M \cdot I(c/s)}{\left(\frac{1}{\cos^2 2a} + \cos^2 2\theta\right) I(eu)}$$

measurements were carried out by step scanning at room temperature between 100° and 160° 2θ. The reported intensity in counts/sec is the measured intensity minus the counter noise (Table 1).

It is believed that the value of K has an accuracy of ±5%.

Table 1

Intensity of Quartz-Standard

2θ	I(c/s)	(μ/ρ)	$\left(\frac{1}{\cos^2 2a} + \cos^2 2\theta\right)$	I(eu)	K
100°	15.70	3.88	1.077	32.45	104.7
110°	16.09	3.91	1.164	31.00	104.5
120°	17.88	3.94	1.297	30.00	108.8
130°	19.65	3.96	1.460	29.20	109.5
140°	22.10	3.98	1.633	28.65	112.9
150°	23.63	4.00	1.797	28.20	112.0
160°	24.56	4.02	1.930	27.85	110.0

Average value of K for $2\theta > 120°$

$$K = \left(111 \pm 5\right)\left(\frac{c/s}{eu}\right)$$

B. Intensity Measurements of Ag_2Al Crystals

One-dimensional measurements were carried out in three directions reciprocal space:

$[110]^*$

$[100]^*$

$[001]^*$, using different crystals.

Along the $[110]^*$ direction the diffuse scattering was considerably stronger than in the other two directions, and showed two marked peaks at 1/3 and 2/3 the distance from the (110) reflection (Figure 6). In this direction the Laue scattering accounted on the average for about 90% of the total diffuse scattering.

The measured intensity values and a detailed calculation of the Laue-diffuse scattering I_S, are given in Table 2.

Measurements were carried out at approximately 300°K and 150°K. The low temperature was obtained by filling the coolant cavity with liquid nitrogen. Assuming a linear variation of the thermal diffuse scattering, it could be eliminated by extrapolation to 0°K.

The results of the intensity measurements along the $[100]^*$ and $[001]^*$ directions are shown in Tables 3 and 4, giving only the final intensity I'_s. Thermal and compton scattering amounted in these two directions up to 50% of the total diffuse scattering.

An interesting observation was made along the $[001]^*$ direction: Superimposed on the diffuse background two peaks occurred at 8.8° and

Table 2

Intensity Measurements Along $[110]$*

2	297°K	I(c/s) 151°K	0°K	$I(\frac{eu}{atom})$	$I_i(\frac{eu}{atom})$	$I_c(\frac{eu}{atom})$	I'_s	h_1
8	10.62	10.60	10.58	89.2	4.7	84.5	0.380	0.096
9	16.64	16.58	16.52	139.8	5.2	134.6	0.620	0.108
10	27.35	27.23	27.11	230.0	5.7	224.3	1.067	0.119
11	33.60	33.03	32.44	276.0	6.2	269.8	1.312	0.131
12	21.20	20.17	19.10	162.9	6.7	156.2	0.786	0.142
13	16.72	15.72	14.69	125.9	7.2	118.7	0.618	0.154
14	16.16	15.51	14.84	127.7	7.6	120.1	0.651	0.165
15	18.52	17.36	16.16	139.5	8.1	131.4	0.739	0.177
16	25.72	25.10	24.46	212.0	8.6	203.4	1.198	0.188
17	47.87	46.75	45.59	397.5	9.0	388.5	2.38	0.200
18	63.52	63.95	64.40	564.0	9.4	554.6	3.53	0.211
19	50.67	49.57	48.57	428.0	9.8	418.2	2.795	0.223
20	37.02	35.94	34.82	308.3	10.2	298.1	2.10	0.235
21	27.95	26.73	25.47	226.9	10.6	216.3	1.593	0.247
22	19.32	18.68	18.02	161.8	11.0	150.8	1.162	0.258
23	14.90	12.68	10.38	93.6	11.2	82.4	0.663	0.270
24	12.91	10.13	7.25	65.9	11.5	54.4	0.456	0.282
25	14.22	9.78	5.19	47.5	11.8	35.7	0.312	0.293
26	25.57	17.22	8.58	79.1	12.2	66.9	0.609	0.305
28.5		(110) reflection						0.333
30.5	39.72	22.76	5.26	50.3	13.3	37.0	0.404	0.355
31	21.02	11.40	1.45	13.9	13.5	0.4	0.004	0.362
32	11.48	6.78	1.92	18.6	13.7	4.9	0.057	0.373
34	7.25	4.28	1.21	11.9	14.2	-2.3	-.029	0.395
36	7.04	4.69	2.26	22.7	14.7	8.0	0.106	0.419
38	9.17	7.81	6.40	65.6	15.2	50.4	0.709	0.442
39	11.54	10.26	8.94	92.6	15.4	77.2	1.113	0.453
40	13.47	12.61	11.72	122.7	15.6	107.1	1.580	0.463

26.5° 2θ (Figure 7), corresponding to (001) and (003) reflections. Although these peaks have an intensity considerably smaller than the short-range order peaks, they are extremely sharp, indicating that they are caused by long-range ordering. By lowering the x-ray tube voltage to 33 kv (below the excitation voltage of the second harmonic), it was definitely established that the peaks were not caused by incomplete removal of the second harmonic.

Using a 0.2°/min. scanning speed and a 1° detector slit, the integrated intensities of the (002), (003), and (004) lines were measured at 132°K (Table 5)

Table 3

Laue-Diffuse Intensity Along $[100]^*$

2θ	I'_s	h_1	
14	0.807	0.86	
15	0.598	0.92	
15.5	0.708	0.95	
16.35	-	1.00	(100) reflection
17.5	1.203	1.07	
18	0.793	1.10	
19	0.531	1.17	
20	0.520	1.22	
21	0.646	1.28	
22	0.730	1.35	
23	0.841	1.41	
24	0.952	1.47	
25	1.133	1.53	
26	1.308	1.58	
27	1.490	1.65	
28	1.682	1.71	
29	1.762	1.76	
30	1.682	1.82	
31	1.675	1.89	
31.5	2.080	1.91	
33.0	-	2.00	(200) reflection.
34.5	0.598	2.09	
35	0.522	2.12	
36	0.546	2.18	

Table 4

Laue-Diffuse Intensity Along [001]*

2θ	I'_s	h_3	
13	0.403	0.75	
14	0.342	0.80	
15	0.028	0.86	
17.5	-	1.00	(002) reflection
20	0.050	1.15	
21	0.018	1.20	
22	0.109	1.26	
23	0.139	1.32	
24	0.175	1.37	
25	0.264	1.43	
26	0.376	1.48	
27	0.537	1.54	
28	0.723	1.59	
29	0.872	1.64	
30	0.721	1.70	
31	0.573	1.76	
32	0.543	1.81	
33	0.821	1.87	
35.4	-	2.00	(004) reflection
38	0.227	2.15	
39	0.061	2.20	
40	0.009	2.25	
41	0.063	2.31	
42	0.109	2.36	

Table 5

Integrated Intensities of (002), (003), (004) Lines

2θ	hkℓ	I(relative)
17.5°	(002)	49.5×10^3
26.5°	(003)	5.1
35.4°	(004)	19.3×10^3

C. Lattice Parameter Measurements

Together with the diffuse intensity measurements, the positions of several low index fundamental lines were obtained (there was no noticable change of position with temperature). Table 6 shows the angular position of the lines and the lattice parameters calculated from them.

Table 6

Lattice Parameters of the Annealed Phase Ag_2Al

hkℓ	2θ	Lattice Parameters
002	17.5°	c = 4.68 A
004	35.4°	
100	16.35°	
200	33.0°	a = 2.89 A
300	50.4°	
110	28.5°	a = 2.89 A
220	59.0°	

ANALYSIS OF RESULTS

The low intensities along $\left[100\right]^*$ and $\left[001\right]^*$ and the two broad peaks along $\left[110\right]^*$ suggest immediately the presence of strong short-range ordering with the tendency to form a two-dimensional superlattice on the $\{001\}$ planes in which each aluminum atom is surrounded by six silver atoms (Figure 8). Since the breadth of the peaks indicates, that the alloy is far from having this perfect long-range ordering, an estimate of the degree of short range order can be obtained by evaluating the intensity distribution in terms of the Cowley-Warren pair-density coefficients. This theory is actually valid only for low degrees of ordering, since one of its basic assumptions is, that pairs with the same interatomic vector are statistically equivalent. Even though in the present case the appearance of two peaks indicates, that this is not the case and that the ordering effects go beyond the first neighbors, there exists at the present time no better theory on intermediate states of ordering.

When carrying out one-dimensional intensity measurements, for example along $\left[110\right]^*$, Equation 7 reduces to the form:

$$I'_s = (h_1 h_1 0) = \sum_{\rho} C_{\ell} \, e^{2\pi i h_1 (\ell + m)} \tag{8}$$

or in terms of the trigonometric functions:

$$I'_s \, (h_1 h_1 0) = \sum_{\rho} \left[A_{\ell} \, \cos 2\pi h_1 (\ell + m) + i B_{\ell} \, \sin 2\pi h_1 (\ell + m) \right] \tag{9}$$

The evaluation of the Fourier coefficients A and B of a one-dimensional series can be carried out easily by means of the computing scheme for 12 ordinates as given for example by Lipka[29].

In order to distinguish between the short range order coefficients of pairs within the same basal plane (n = 0) and in different basal planes, the former shall be designated by $\alpha_{\ell\ mn}$ and the latter by $\gamma_{\ell\ mn}$.

Using this terminology, the short range order coefficients are related to the calculated Fourier coefficients by:

$$A_\ell + B_\ell = \sum_m \sum_n (\alpha_{\ell\ mn} + \gamma_{\ell\ mn}) \tag{10}$$

The inter-atomic distance r in a hexagonal close-packed lattice with ideal c/a ratio is given by:

$$r/a = \sqrt{\frac{1}{9}(\ell^2 + m^2 - \ell m) + \frac{2}{3} n^2}$$

The first few interatomic pair distances and their corresponding short range-order coefficients are given in Table 7.

Table 7

Interatomic Pair Distances and Their Short Range Order Coefficients

r/a	α_i	ℓ mn	r/a	γ_i	ℓ mn
0	0	000			
1.00	1	300	1.00	1	121
		330			$\bar{2}\bar{1}1$
		030			$1\bar{1}1$
1.73	2	630	1.41	2	421
		360			$\bar{2}\bar{4}1$
		$3\bar{3}0$			$\bar{2}21$
2.0	3	600	1.63	3	002
		660			
		060			

Using the values of I'_s given in Table 2, Figure 9 was plotted, and from this graph the Fourier-coefficients were evaluated by means of a 12-ordinate scheme (Table 8).

Table 8

Intensity Distribution Along $\left[110\right]^*$ and the Fourier-Coefficients

h_1	s	I'_s		
0.028	1	-	$A_0 = +0.76$	
0.056	2	-	$A_1 = -0.73$	$B_1 = -0.70$
0.083	3	-	$A_2 = -0.25$	$B_2 = +0.35$
0.111	4	0.70	$A_3 = +0.40$	$B_3 = +0.04$
0.139	5	0.90	$A_4 = -0.22$	$B_4 = -0.13$
0.167	6	0.65	$A_5 = +0.00$	$B_5 = +0.09$
0.195	7	1.80	$A_6 = +0.04$	
0.222	8	2.90		
0.250	9	1.40		
0.278	10	0.55		
0.306	11	0.15		
0.333	12	0.00		
0.362	1	0.00		
0.389	2	0.00		
0.417	3	0.10		

Table 9 shows the results of the equivalent evaluations for the $\left[100\right]^*$ and $\left[001\right]^*$ directions. As given by Equation (10), the short-range order coefficients can now be calculated from the Fourier-coefficients according to Table 10, neglecting terms beyond α_3 and γ_3.

Table 9

Fourier-Coefficients Along $[100]^*$ and $[001]^*$

$[100]^*$		$[001]^*$	
$A_0 = +0.95$		$A_0 = +0.24$	
$A_1 = -0.26$	$B_1 = -0.50$	$A_1 = -0.28$	$B_1 = -0.20$
$A_2 = -0.22$	$B_2 = +0.03$	$A_2 = -0.02$	$B_2 = +0.16$
$A_3 = -0.05$	$B_3 = +0.10$	$A_3 = +0.08$	$B_3 = -0.03$
$A_4 = +0.02$	$B_4 = +0.07$	$A_4 = -0.02$	$B_4 = -0.03$
$A_5 = +0.04$	$B_5 = +0.03$	$A_5 = -0.01$	$B_5 = +0.02$
$A_6 = +0.02$		$A_6 = 0.00$	

The resulting short-range order coefficients are as follows:

$\alpha_1 = -0.17$	Symmetric and anti-symmetric
$\alpha_2 = +0.10$	Symmetric
$\alpha_3 = -0.17$	Symmetric and anti-symmetric
$\gamma_1 = -0.19$	Symmetric and anti-symmetric
$\gamma_2 = +0.04$	Anti-symmetric
$\gamma_3 = +0.08$	Anti-symmetric

Table 10

Relationships Between Fourier-Coefficients and Short-Range Order Parameters

$[110]^*$	$A_1 + B_1 = 4\alpha_1 + 4\gamma_1$
	$A_2 + B_2 = 2\alpha_1 + 4\alpha_3 + 4\gamma_2$
	$A_3 + B_3 = 4\alpha_2$
	$A_4 + B_4 = 2\alpha_3$
$[100]^*$	$A_1 + B_1 = 4\gamma_1$
	$A_2 + B_2 = 2\gamma_1 + 4\gamma_2$
	$A_3 + B_3 = 4\alpha_1 + 4\alpha_2$
	$A_4 + B_4 = 2\gamma_2$
$[001]^*$	$A_1 + B_1 = 6\gamma_1 + 6\gamma_2$
	$A_2 + B_2 = 2\gamma_3$

For the proposed model of a two-dimensional superlattice the α's for complete order would be:

$\alpha_1 = -0.50$	Symmetric and anti-symmetric
$\alpha_2 = +1.00$	Symmetric
$\alpha_3 = -0.50$	Symmetric and anti-symmetric

In this connection the expression "symmetric" means, that corresponding positive and negative interatomic vectors are of the same type, either connecting like or unlike atoms, while "anti-symmetric" means that the vectors are of the opposite type.

While the short-range order parameters in the basal plane indicate, that the proposed model for the atomic arrangement within the basal planes is

correct, no prediction can be made as to the expected stacking of these identical layers in a three-dimensional superlattice. There are two extreme cases one can visualize: atoms in equivalent positions in alternate layers could be either of the same or the opposite type. It will require the attainment of long-range order to decide this question.

Whatever the stacking sequence however, there is no possibility for the formation of (001) superlattice lines, as observed in the present investigation. These lines can only be caused by a regular composition difference between consecutive layers. An estimate of this composition difference can be made by comparison of the integrated intensity of the superlattice line with that of a fundamental line.

Assuming that the stochiometric compound Ag_2Al contains a slight excess "x" of aluminum, for example, and that this excess goes regularly into alternate basal planes throughout the diffracting volume of the crystal, the ratio of the intensity of the (003) superlattice line to that of fundamental lines of the same form is given by:

$$\frac{I_S}{I_F} = \frac{9\,x^2\,(f_{Ag} - f_{Al})^2}{(2\,f_{Ag} + f_{Al})^2} \qquad \frac{(1 + \cos^2 2\theta_S)\,(\sin 2\theta_F)}{(1 + \cos^2 2\theta_F)\,(\sin 2\,\theta_S)}$$

neglecting temperature and extinction effects.

Using the measured intensity values of Table 5, x = 1.6% by comparison with the (002) line and 1.2% by comparison with the (004) line. The higher value of x for the (002) reflection is very likely due to primary extinction.

Again, the final explanation for the presence of long-range order together with short-range order, requires more work, directed particularly toward the effects of heat treatment and composition on ordering.

One of the physical properties that depend on the atomic arrangement and that can be measured easily are the lattice parameters. The values reported in Table 6, $a = 2.89$ Å are believed to be precise to ±0.02Å and $c = 4.615$ Å

it is interesting to compare them to values reported by Massalski[30] on quenched samples of this alloy: $a = 2.878$ Å
$c = 4.615$ Å

Massalski's a-parameter is within the accuracy of the present determination but the difference between the c-parameters is significant enough to conclude, that the atomic arrangement in this alloy is quite different in the quenched and annealed state.

The same model for a superlattice as proposed in the present investigation was reported by Guinier[31] for metastable Guinier - Preston zones below 150°C in the aluminum-rich δ-phase in the system silver-aluminum. Even though the disappearance of the superlattice lines at 160°C in Guinier's work seems to be caused by a change in the composition of the zones[32], it might be interesting to lower the annealing temperature of the alloy Ag_2Al also to 140°C, in an attempt to establish long-range order.

CONCLUSIONS

The alloy Ag_2Al, when annealed for several days at 450°K, shows strong short range ordering. Position and intensity of the short-range orderpeaks indicate a tendency to form a superlattice on the basal planes, in which each aluminum atom is surrounded by six silver atoms. No prediction can be made concerning the expected stacking sequence of these basal planes in the three-dimensional superlattice.

Very faint but sharp diffraction lines of the type (001), (003) must be due to a systematic composition difference of consecutive basal planes; the sharpness of the lines indicates that it is a long-range ordering effect.

A comparison of the lattice parameters of the annealed alloy with parameters obtained from the quenched alloy shows, that the c-parameter in the annealed state is 0.06 A larger than in the quenched state, indicating a large change in the atomic arrangement.

ACKNOWLEDGMENTS

The author would like to express his gratitude to Professor J.E. Dorn for the advice and encouragement he has given during this work.

Furthermore, he would like to thank Professor F.E. Hauser for help in the design of the diffraction chamber and Mr. R. Collins for the outstanding workmanship in the construction of crystal monochromator and diffraction chamber.

This work was done under the auspices of the U.S. Atomic Energy Commission.

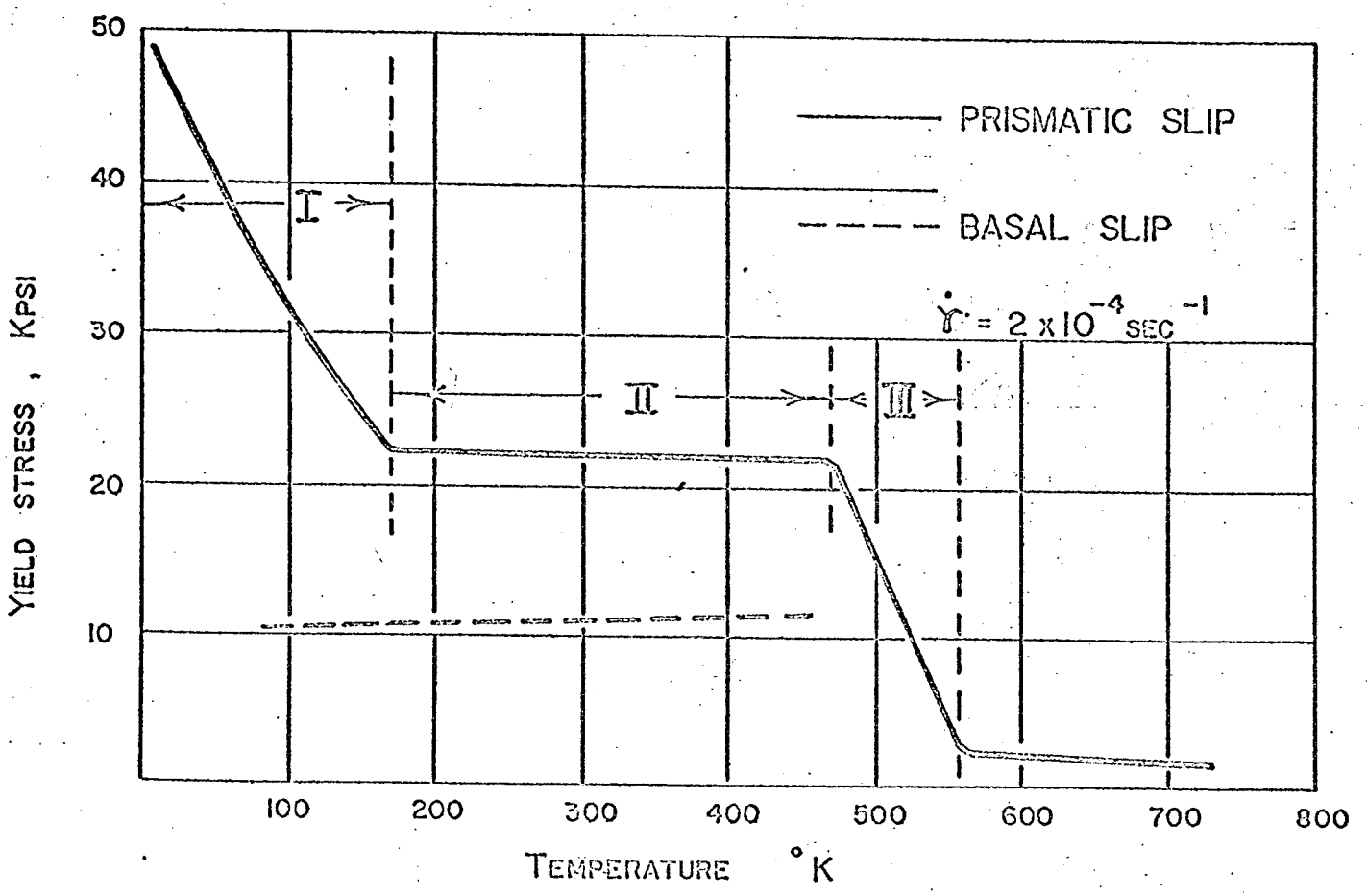

Fig. 1. YIELD STRESS FOR PRISMATIC AND BASAL SLIP AS A FUNCTION OF TEMPERATURE FOR THE HEXAGONAL INTERMETALLIC COMPOUND Ag_2Al.

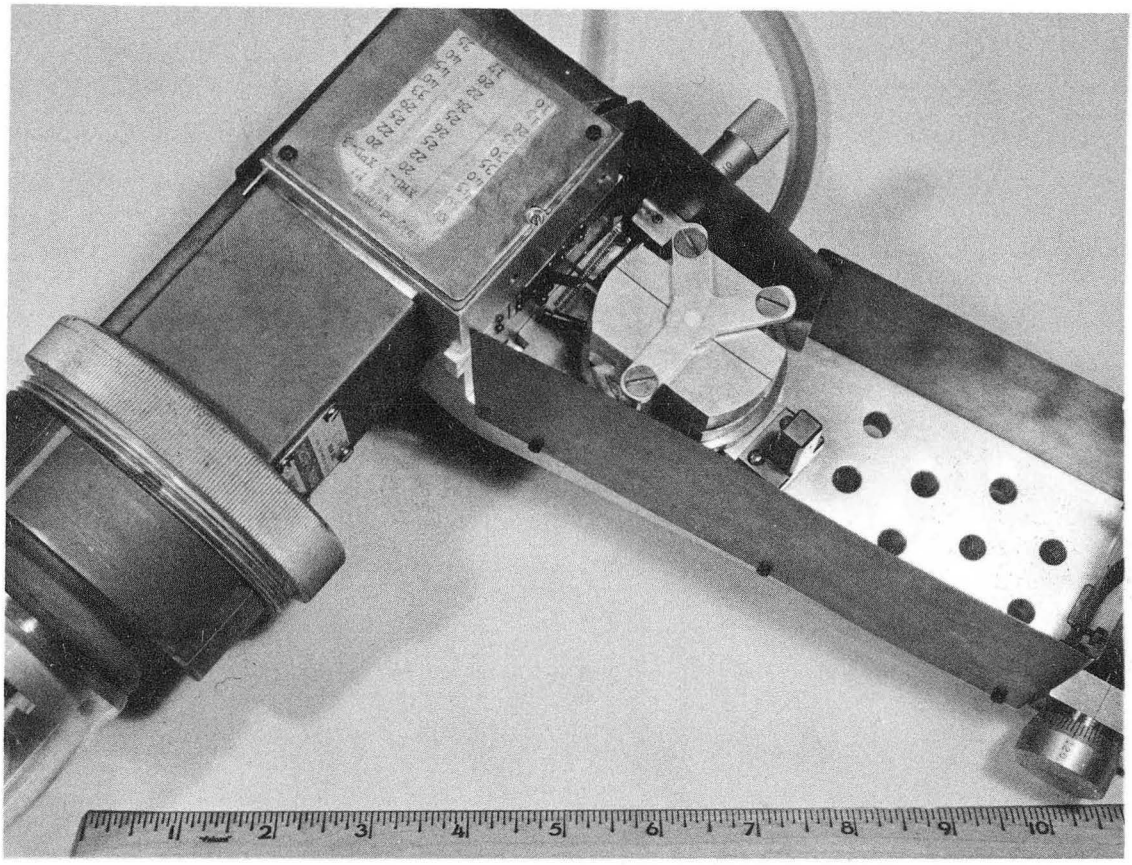

ZN-4697

Fig. 2

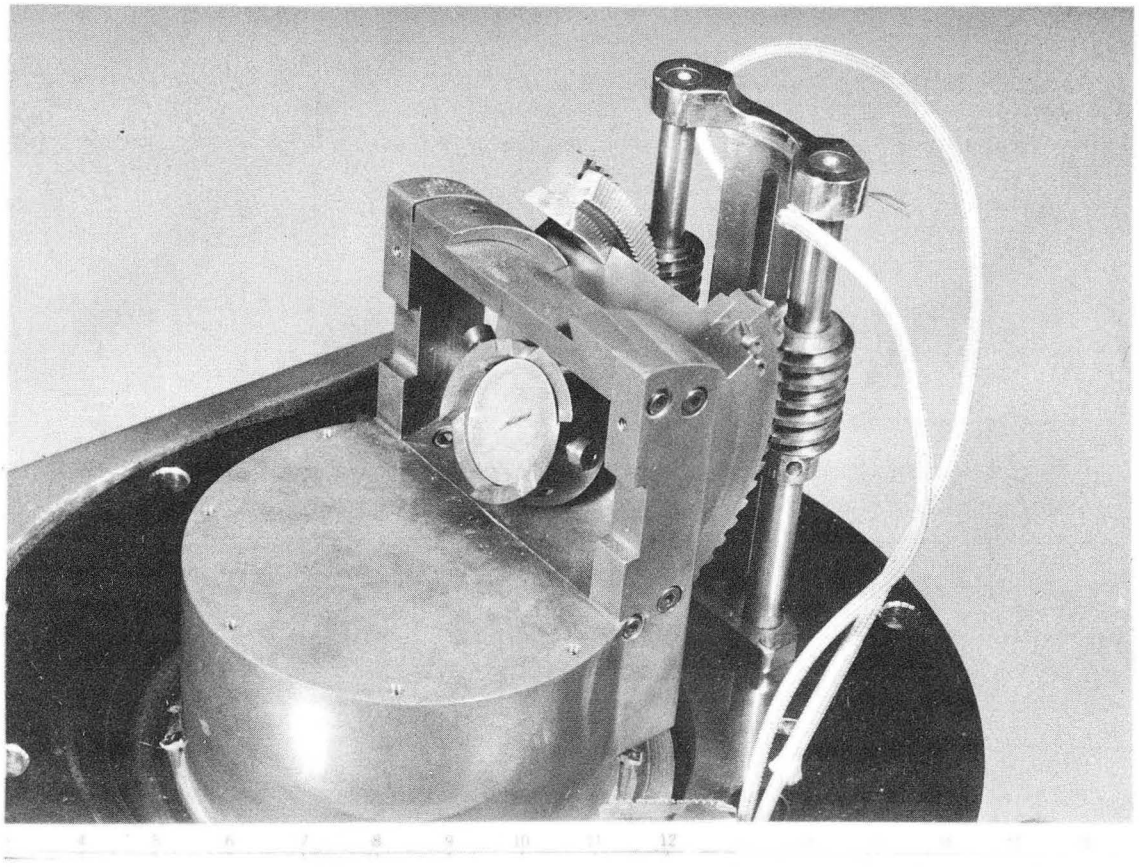

ZN-4698

Fig. 3

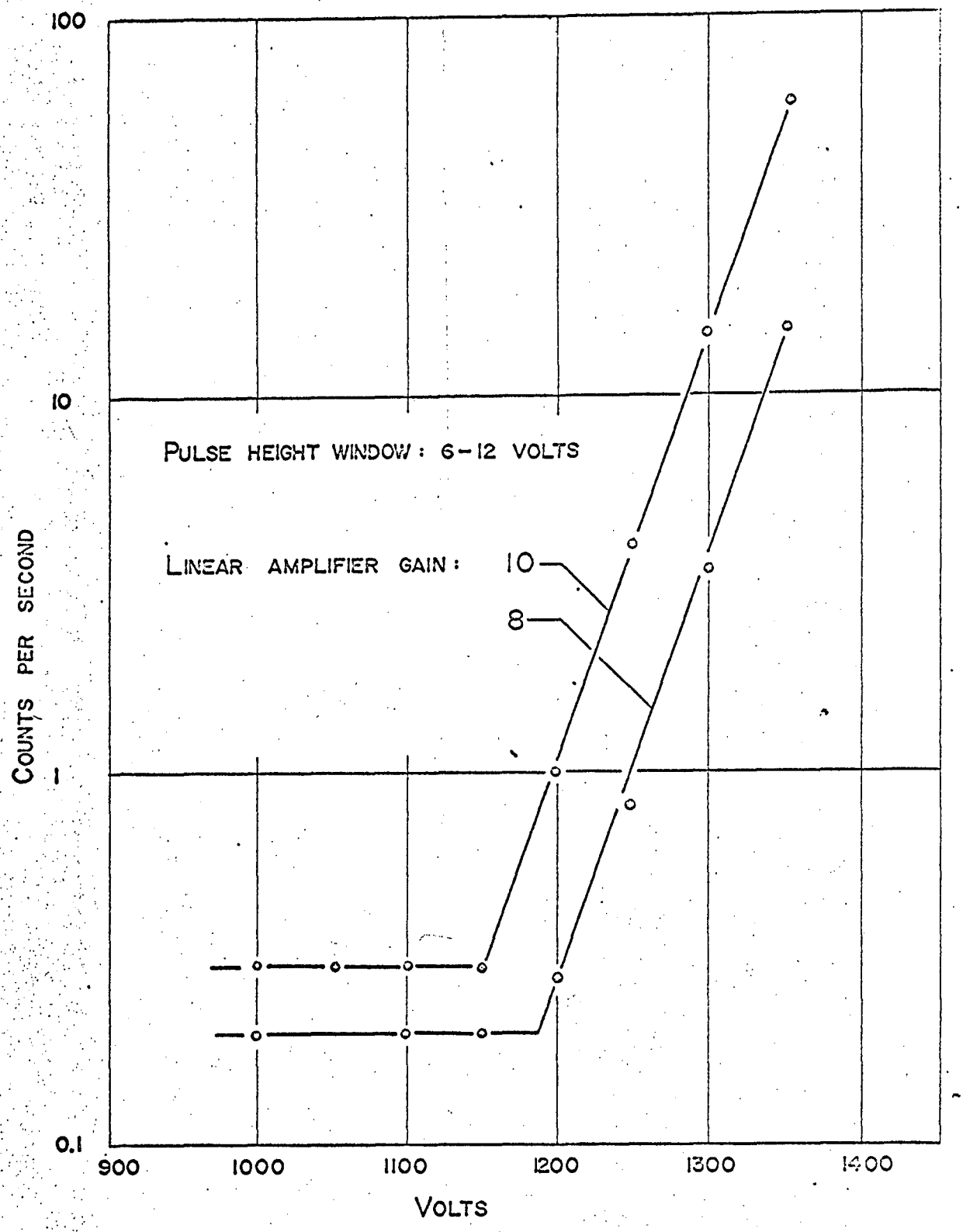

Fig. 4. NOISE LEVEL OF SCINTILLATION COUNTER AS A FUNCTION OF PHOTOMULTIPLIER VOLTAGE

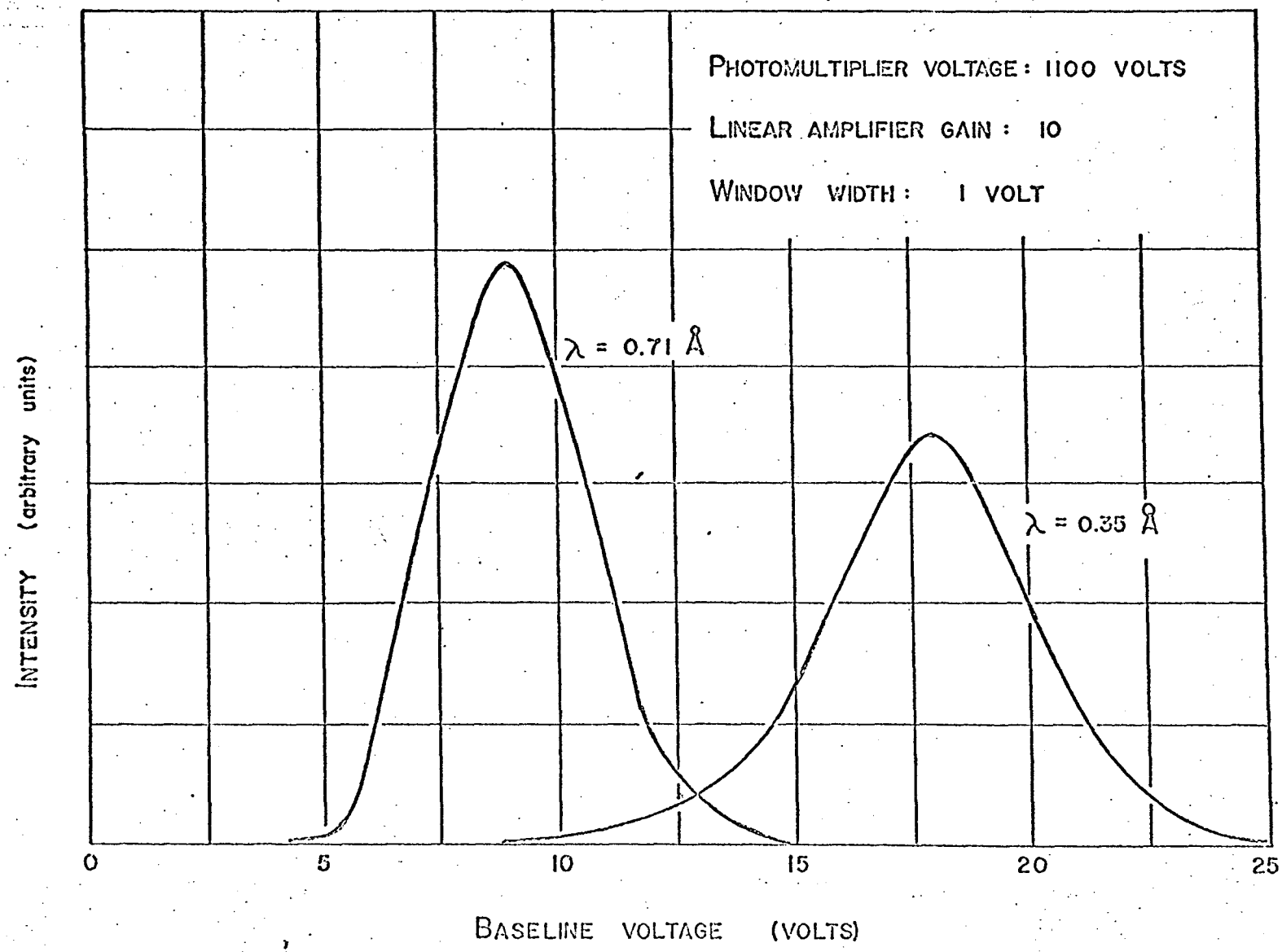

Fig. 5. PULSE-HEIGHT DISTRIBUTION OF $Mo - K_\alpha$ RADIATION AND ITS SECOND HARMONIC

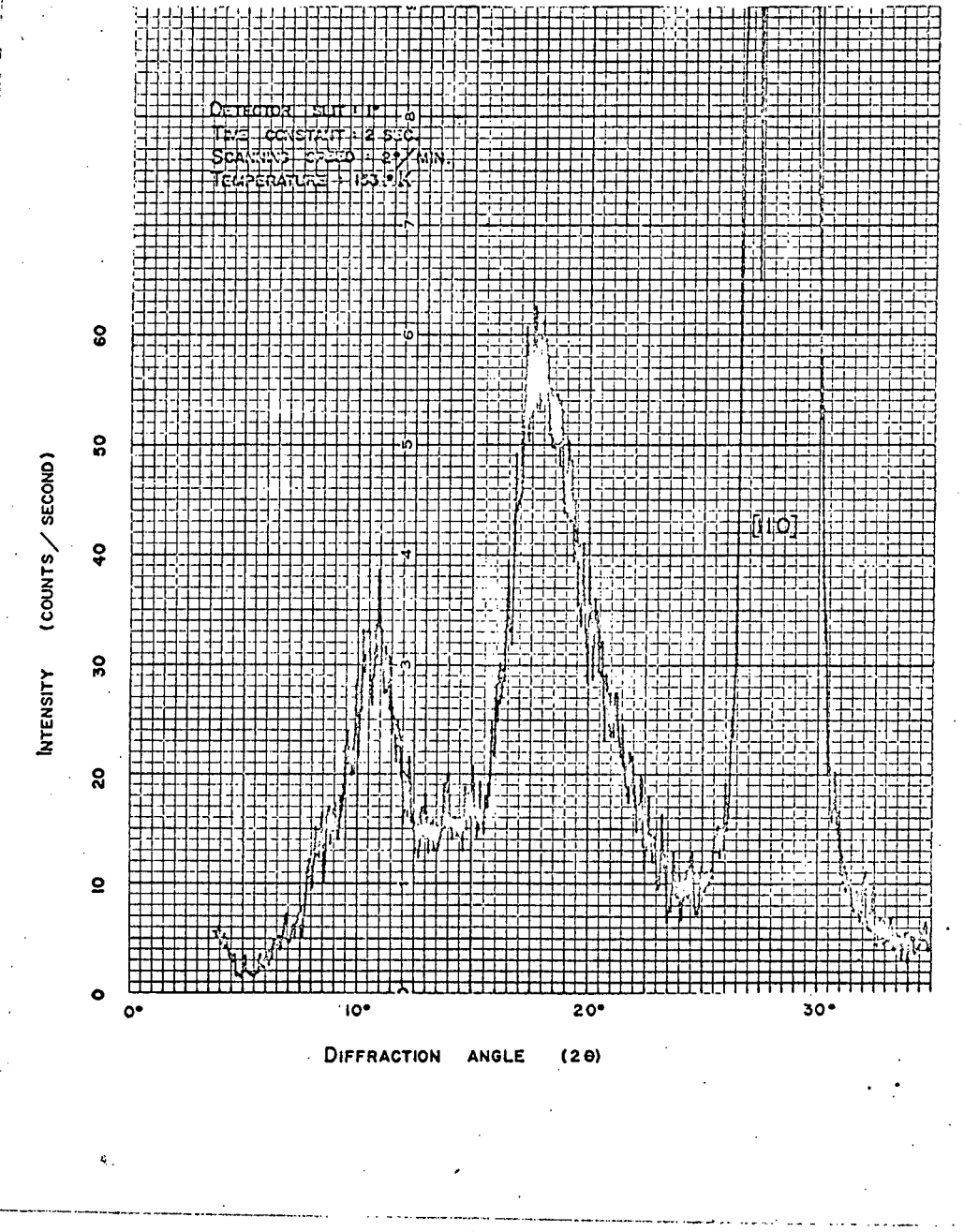

Fig. 6. Ag_2Al SINGLE CRYSTAL INTENSITY ALONG [110]*

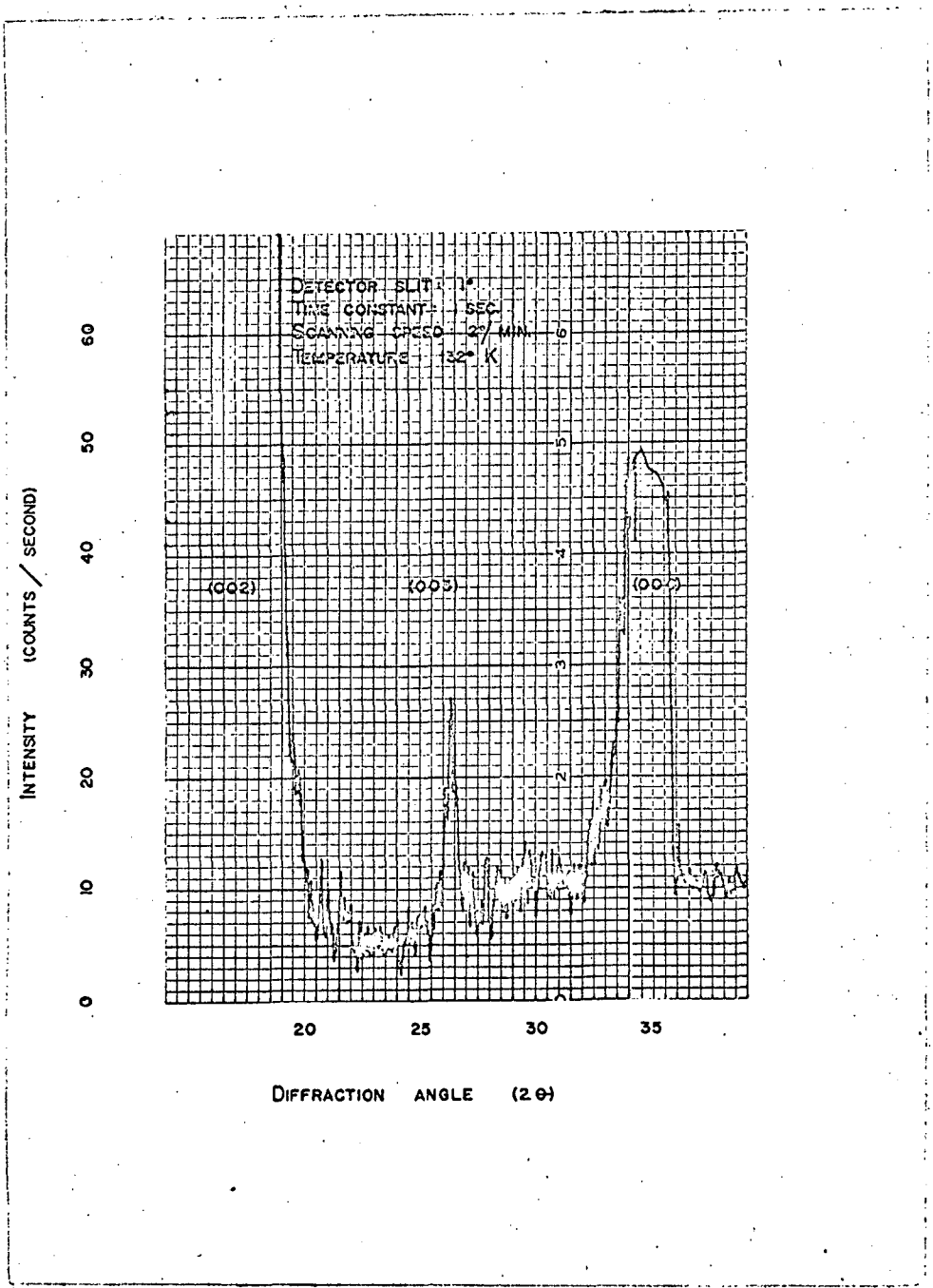

Fig. 7. Ag_2Al SINGLE CRYSTAL INTENSITY ALONG [001]*

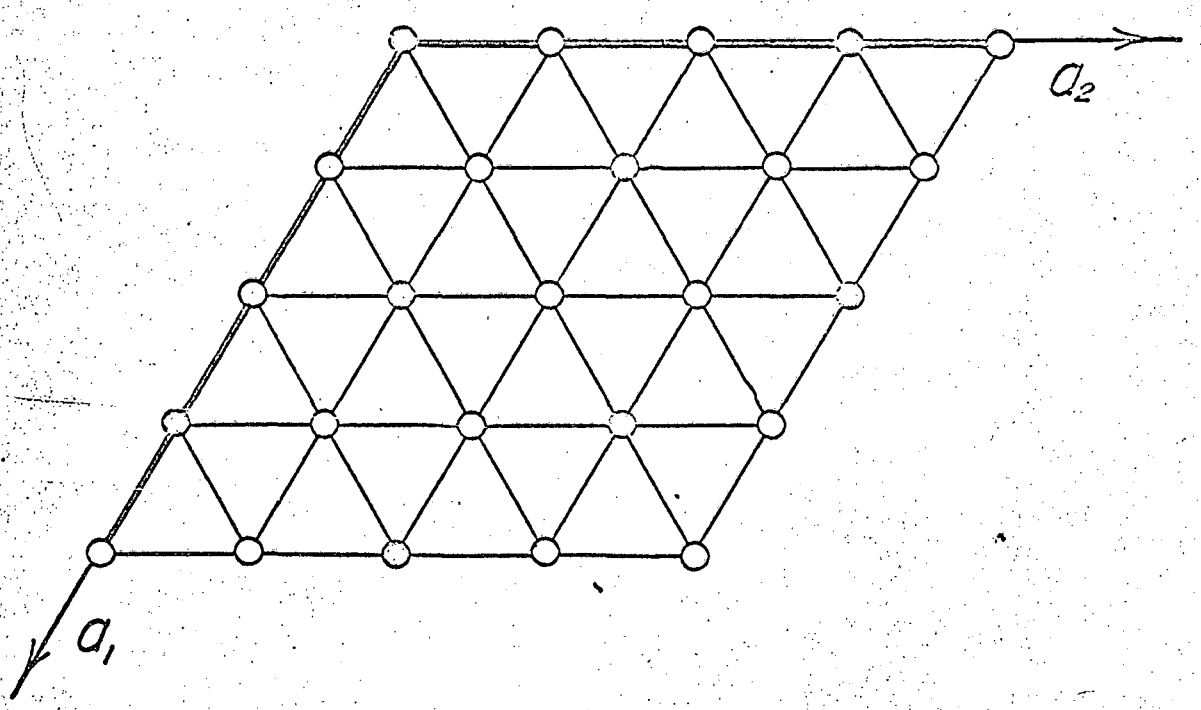

○ ALUMINUM

○ SILVER

Fig. 8. MODEL OF SUPER LATTICE IN BASAL PLANES

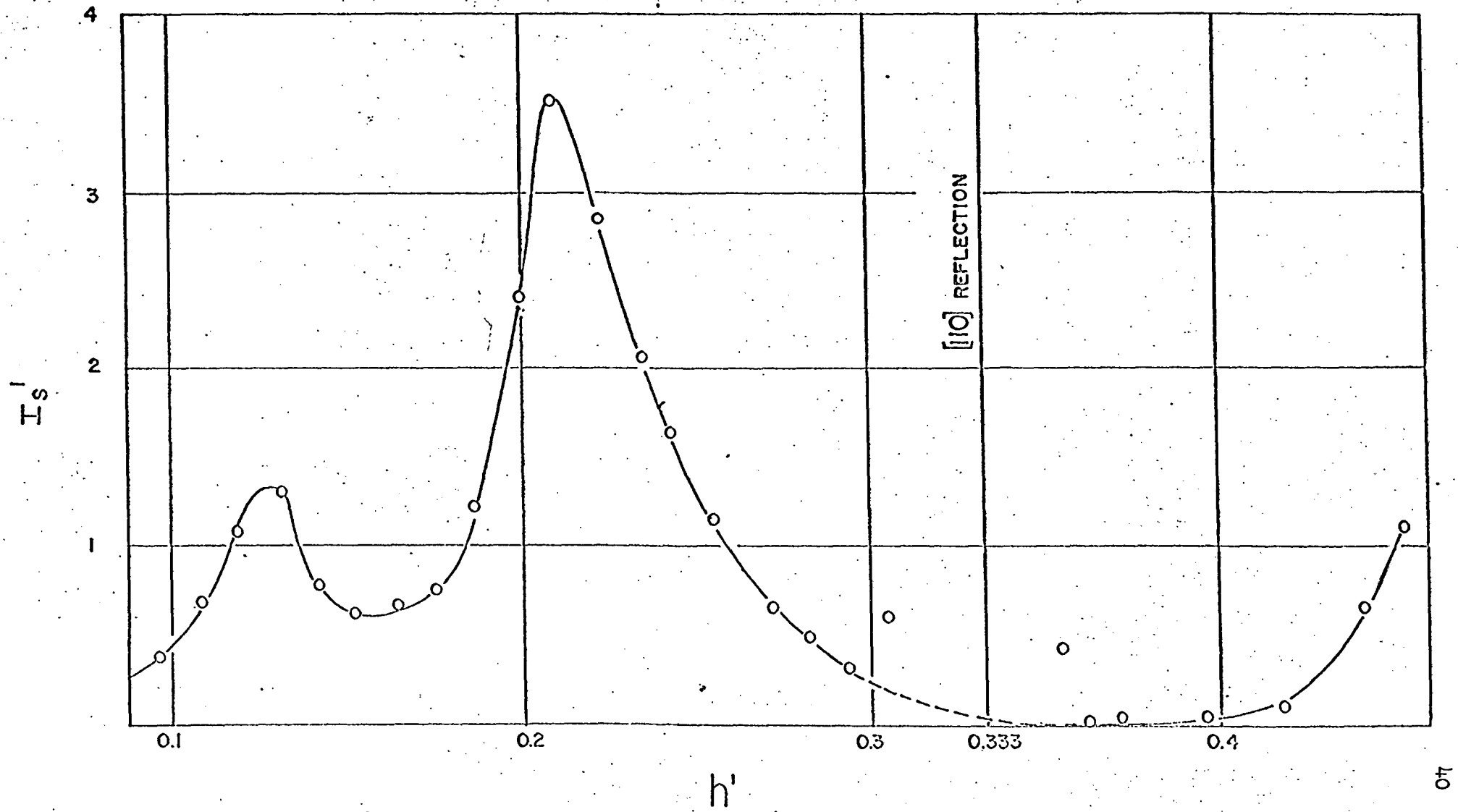

Fig. 9. LAUE-DIFFUSE INTENSITY ALONG [110]*

APPENDIX I

DIFFRACTION THEORY

The amplitude of a plane wave scattered at a point p, whose position relative to a convenient origin is given by the vector $\vec{r}_p$ is according to Laue[18]:

$$A = \text{const } e^{2\pi i \left[\nu t - \frac{1}{\lambda} \vec{r}_p (\vec{s}-\vec{s}_0) \right]}$$

where

$\vec{s}_0$ = direction of incident beam

$\vec{s}$ = direction of scattered beam

λ = wavelength of radiation

ν = frequency of radiation

If the angle between incident and scattered beam is 2θ,

$$(\vec{s} - \vec{s}_0) = 2 \sin \theta$$

In an assembly of scattering points, the resulting amplitude is the sum over all points:

$$A = \text{const} \sum_p e^{2\pi i \left[\nu t - \frac{1}{\lambda} \vec{r}_p (\vec{s}-\vec{s}_0) \right]}$$

The resulting intensity is given by A^2 and is obtained by multiplication with the complex conjugate:

$$I = |A|^2 = \text{const} \sum_p \sum_q \ell^{\frac{2\pi i}{\lambda} (\vec{r}_q - \vec{r}_p)(\vec{s}-\vec{s}_0)}$$

Expressing the intensity scattered by one electron by Thomson's equation[20]:

$$I_e = \frac{\text{const}}{R^2} \quad \frac{1 + \cos^2 2\theta}{2} \; I_0$$

where I_0 the intensity of the incident unpolarized wave and R the distance from the scattering point, the intensity scattered by an assembly of electrons within an atom in terms of I_e is:

$$I = I_e \sum_p \sum_q e^{\frac{2\pi i}{\lambda} (\vec{r}_q - \vec{r}_p)(\vec{s} - \vec{s}_0)}$$

Applying this to an assembly of N atoms, where the p's and q's atoms scatter with an amplitude f_p and f_q, the resulting intensity is given by:

$$I = I_e \sum_{p=1}^{N} \sum_{q=1}^{N} f_p f_q \, e^{\frac{2\pi i}{\lambda} (\vec{r}_q - \vec{r}_p)(\vec{s} - \vec{s}_0)}$$

Assuming that this assembly of N atoms contains two types of atoms[19][21], A and B, there can be found N pairs with the same interatomic vector $(\vec{r}_q - \vec{r}_p) = \vec{r}_{pq}$, with three types of pairs being possible for the same vector $\vec{r}_{pq}$: the vector can connect an A-A, B-B, or A-B pair.

If $P_{AA}(\vec{r}_{pq})$, $P_{BB}(\vec{r}_{pq})$ $P_{AB}(\vec{r}_{pq})$ are the pair density functions or the probabilities of finding an A-A, B-B, A-B (or B-A) pair connected by the vector $\vec{r}_{pq}$, the intensity for a certain diffraction vector $(\vec{s} - \vec{s}_0)$, is given by:

$$I(\vec{s} - \vec{s}_0) = I_e \sum_{p=1}^{N} \sum_{q=1}^{N} (N p_{AA} f_A^2 + N p_{BB} f_B^2 + N p_{AB} f_A f_B) + e^{\frac{2\pi i}{\lambda} \vec{r}_{pq} (\vec{s} - \vec{s}_0)}$$

where it is assumed, that the observed intensity-value is equal to the value obtained by averaging over all the actually existing pair-densities, i.e., that the interatomic vectors are statistically equivalent, which will actually be true only for solutions with a low degree of order. For a binary solution this can be simplified since there is only one independent pair-density function, which suffices to define the state of order in the alloy. With x_A and x_B being the atomic fractions of component A and B, respectively; P_{AA} as well as P_{BB} can be expressed in terms of P_{AB}[21]:

$$P_{AA} = x_A - \frac{P_{AB}}{2} \quad ; \quad P_{BB} = x_B - \frac{P_{AB}}{2}$$

and

$$I = I_e N \sum_{p=1}^{N} \sum_{q=1}^{N} \left[x_A f_A^2 + x_B f_B^2 - \frac{1}{2} P_{AB} (f_A - f_B)^2 \right] e^{\frac{2\pi i}{\lambda} \vec{r}_{pq} (\vec{s} - \vec{s}_0)}$$

This equation gives the total intensity of the radiation coherently scattered by a crystal with the atoms at rest.

It can be separated into terms that contain P_{AB}, i.e., they depend on the state of order, and terms, that do not contain P_{AB}.

$$\frac{I}{N I_e} = \sum\sum \left[x_A f_A^2 + x_B f_B^2 \right] e^K + \sum\sum \left[- \frac{P_{AB}}{2} (f_A - f_B)^2 \right] e^K$$

with

$$K = \frac{2\pi i}{\lambda} \vec{r}_{pq} (\vec{s} - \vec{s}_0)$$

Substracting from the 1st sum $x_A x_B (f_A - f_B)^2$ and adding it to the second:

$$\frac{I}{NI_e} = \sum \left[x_A f_A^2 + x_B f_B^2 - x_A x_B (f_A - f_B)^2 \right] e^K$$

$$+ \sum \left[x_A x_B (f_A - f_B)^2 - \frac{P_{AB}}{2} (f_A - f_B)^2 \right] e^K$$

therefore:

$$\frac{I}{NI_e} = \sum (x_A f_A + x_B f_B)^2 e^K + \sum (f_A - f_B)^2 \left[1 - \frac{P_{AB}}{2 x_A x_B} \right] e^K$$

APPENDIX II

RECIPROCAL LATTICE OF THE HEXAGONAL SYSTEM

The reciprocal lattice of any crystal lattice is defined by: (all quantities in reciprocal space are marked with an asterisk).

The Directions of the reciprocal lattice axes:

$\vec{a}_1^*$ is perpendicular to $\vec{a}_2$ and $\vec{c}$

$\vec{a}_2^*$ is perpendicular to $\vec{a}_1$ and $\vec{c}$

$\vec{c}^*$ is perpendicular to $\vec{a}_1$ and $\vec{a}_2$

The lengths of the reciprocal lattice axes:

$$a_1^* = \frac{1}{V}(\vec{a}_2 \times \vec{c})$$

$$a_2^* = \frac{1}{V}(\vec{a}_1 \times \vec{c})$$

$$c^* = \frac{1}{V}(\vec{a}_1 \times \vec{a}_2)$$

V is the volume of the crystal-lattice unit cell; for the hexagonal system:

$$V = a_1 \cdot a_2 \cdot c \cdot \cos 30$$

The vector product of two vectors is given by:

$$\vec{a}_2 \times \vec{c} = a_2 \cdot c \cdot \sin \alpha_1$$

$$\vec{a}_1 \times \vec{c} = a_1 \cdot c \cdot \sin \alpha_2$$

$$\vec{a}_1 \times \vec{a}_2 = a_1 \cdot a_2 \cdot \sin \gamma$$

α_1: angle between $\vec{a}_2$ and $\vec{c} = 90°$

α_2: angle between $\vec{a}_1$ and $\vec{c} = 90°$

γ : angle between $\vec{a}_1$ and $\vec{a}_2 = 120°$

The crystal lattice axes and the reciprocal lattice axes have the property that

$$\vec{a}_m \cdot \vec{a}_n^* = 0 \qquad \text{when } m \neq n$$

$$= 1 \qquad \text{when } m = n$$

APPENDIX III

COMPUTATION OF THE INTENSITY IN ELECTRON UNITS SCATTERED BY SiO_2

For a material of low atomic number, at high diffraction angles, each atom can be assumed to scatter independently. Taking the molecular unit of quartz-glass as SiO_2, the scattered intensity is given by:

$$I^{SiO_2}(eu) = I_c^{Si} + I_i^{Si} + 2\,I_c^{O} + 2\,I_i^{O}$$

The superscripts refer to the type of atom, the subscripts to coherent and incoherent radiation respectively. The computation of the coherent intensity is given in the following table; the atomic scattering factors were taken from the International Tables[16]. Since Mo-K_α-radiation was used, the scattering factor of silicon was corrected for dispersion, neglecting the imaginary part of the anomalous scattering factor and taking $\Delta f'$ independent of the angle as $+0.1$[17].

Coherent intensity of SiO_2:

$\sin\theta/\lambda$	0.9	1.0	1.1	1.2	1.3	1.4
f_0(Oxyg)	1.462	1.374	1.296	1.220	1.144	1.070
$I_c^0 = f^2$	2.14	1.89	1.68	1.49	1.31	1.15
f_0 (Si)	3.16	2.69	2.35	2.07	1.87	1.71
$(f_0 + \Delta f')$	3.26	2.79	2.45	2.17	1.97	1.81
$I_c^{Si} = f^2$	10.62	7.78	6.00	4.70	3.88	3.27
ΣI_c	14.90	11.56	9.36	7.68	6.50	5.57

The incoherent intensity was computed from the ground state-calculations for oxygen by Milberg and Brailsford[22] and for silicon by Freeman[23]. In both cases the relativistic Breit-Dirac correction was applied (Appendix IV). The following table gives the values for the incoherent intensity as well as its fraction of the total intensity. This latter value is important when selecting the mass-absorption coefficient (Appendix V).

$\sin\theta/x$	0.9	1.0	1.1	1.2	1.3	1.4
I_i^0	6.750	6.894	7.025	7.148	7.259	7.361
$I_i^0 \cdot R$	6.22	6.23	6.22	6.18	6.12	6.05
I_i^{Si}	10.82	11.25	11.59	(11.9)	(12.1)	(12.3)
$I_i^{Si} \cdot R$	9.97	10.18	10.26	10.30	10.22	10.1
$\Sigma I_i \cdot R$	22.41	22.64	22.70	22.66	22.46	22.20
ΣI_c	14.90	11.56	9.36	7.68	6.50	5.57
ΣI(eu)	37.31	34.20	32.06	30.34	28.96	27.77
$I_i/\Sigma I$	.60	.66	.71	.75	.78	.80

APPENDIX IV

RELATIVISTIC BREIT-DIRAC-CORRECTION MoK_a-RADIATION

Relativistic Breit-Dirac-correction for MoK_a-radiation. The inelastic or Compton scattering of an x-ray quantum by an electron causes an increase of the wavelength given in its simplest form by:

$$\Delta\lambda \left[\text{Å}\right] = 0.0242\ (1 - \cos 2\theta)$$

Actually the incoherent radiation forms a band and the Compton formula applies to the peak of this band. The formula neglects furthermore the defect-shift[24], which results in a wavelength-shift a few percent less than the one predicted by this formula.

As a consequence of the wavelength-shift, the intensity of the incoherent radiation is lowered by the Breit-Dirac-factor R, where $R = \frac{-1}{B^3}$ and

$$B = \left[1 + 0.0242 \cdot 2\lambda \left(\frac{\sin\theta}{\lambda}\right)^2\right]$$

For MoK_a-radiation ($\lambda = 0.71$ A), the B-D-factor is given as a function of $\frac{\sin\theta}{\lambda}$ in the following table:

$\frac{\sin\theta}{\lambda}$	0.1	0.2	0.3	0.4	0.5	0.6	0.7
R	0.999	0.996	0.990	0.983	0.975	0.964	0.951
$\frac{\sin\theta}{\lambda}$	0.8	0.9	1.0	1.1	1.2	1.3	1.4
R	0.937	0.921	0.904	0.885	0.865	0.844	0.822

APPENDIX V

EFFECTIVE MASS-ABSORPTION COEFFICIENT OF SiO_2

When computing $(\frac{\mu}{\rho})$ for SiO_2 one has to take into consideration the fact that part of the scattered radiation - the incoherent radiation - has a longer wavelength ($\lambda_i = \lambda_c + \Delta\lambda$) than the coherent Mo-$K_\alpha$ radiation λ_c and therefore a higher absorption coefficient μ_i.

For the wavelength region of $\lambda \simeq 0.7$ Å the absorption coefficients of oxygen and silicon follow approximately a λ^3 law[15], so that:

$$\frac{\mu_i}{\mu_c} = \left(\frac{\lambda_i}{\lambda_c}\right)^3 \quad ; \quad \text{and} \quad \mu_i = \mu_c \left(1 + \frac{\Delta\lambda}{\lambda_c}\right)^3$$

which can be approximated by:

$$\mu_i \simeq \mu_c \left(1 + \frac{3\Delta\lambda}{\lambda}\right) \quad ; \quad \text{since} \quad \frac{\Delta\lambda}{\lambda} << 1$$

For the incoherent part of the scattered radiation, the absorption coefficient should be taken as the average of μ_i and μ_c:

$$\overline{\mu} = \mu_c \left[1 + \frac{3}{2}\left(\frac{\Delta\lambda}{\lambda}\right)\right]$$

With:

$$\Delta\lambda = 0.0242\ (1 - \cos 2\theta)$$

$$\overline{\mu} = \mu_c \left[1 + 0.0511\ (1 - \cos 2\theta)\right]$$

Using the values for the fraction of incoherent radiation given in Appendix III, $\mu_{effective}$ can be calculated:

$$\mu_{eff} = \overline{\mu}\ \frac{I_i}{\Sigma I} + \mu_c \left(1 - \frac{I_i}{\Sigma I}\right)$$

Effective Mass-Absorption Coefficient

2θ	90	100	110	120	130	140	150	160
$\bar{\mu}/\mu_c$	1.051	1.060	1.069	1.077	1.084	1.090	1.095	1.099
$\frac{I_i}{\Sigma I}$	0.66	0.70	0.73	0.76	0.77	0.78	0.79	0.80
$\frac{\mu_{eff}}{\mu_c}$	1.034	1.042	1.050	1.058	1.065	1.070	1.075	1.079

This correction is by no means negligible, ranging from 3% at $2\theta = 90°$ to 8% at 160°.

With the values of $\frac{\mu}{\rho}$ for oxygen and silicon for $\lambda_c = 0.71$ Å given in the Intern. Tables[14],

$$\left(\frac{\mu}{\rho}\right)_{SiO_2} = 3.72 \ \frac{cm^2}{g}$$

Molecular-unit weight $M_{SiO_2} = 60.1$. No corrections of the absorption coefficient were made for the absorption in the 10 cm air path, the 0.015" beryllium window in the vacuum chamber and the 0.005" beryllium window in the counter, since the transmission for these is 98%.

APPENDIX VI

INCOHERENT SCATTERING OF ALUMINUM AND SILVER

The incoherent scattering of aluminum was taken from the calculations by Freeman[25]; for lower angles the experimental values by Laval[26] were used. It is shown - including the Breit-Dirac correction - in the following table.

Incoherent Scattering of Aluminum

$\frac{\sin\theta}{\lambda}$	0.1	0.15	0.2	0.3	0.4	0.5
$I_i \cdot R\ (\frac{eu}{atom})$	1.2	2.4	3.5	5.2	6.3	7.3
$\frac{\sin\theta}{\lambda}$	0.6	0.7	0.8	0.9		
$I_i \cdot R$	8.1	8.7	9.1	9.4		

Since no newer calculations of the incoherent scattering of silver are available, the Heisenberg-Bewilogua computation method was used[27][28].

Based on a Thomas-Fermi distribution, Heisenberg gives $I_i(eu)$ as:

$$I_i(eu) = Z \cdot s(v)$$

where

$$v = \frac{4\pi \sin\theta}{\lambda} \cdot \frac{0.176}{z^{2/3}}$$

with z(atomic number) = 47 for silver,

$$v = 0.170 \cdot \frac{\sin\theta}{\lambda}$$

Using the numerical evaluation of s(v) by Bewilogua, the following values are obtained.

Incoherent Scattering of Silver

$\frac{\sin\theta}{\lambda}$	v	s	$I_i \cdot R(\frac{eu}{atom})$
0.1	0.017	0.14	6.6
0.15	0.025	0.19	8.9
0.2	0.034	0.245	11.5
0.3	0.051	0.32	14.9
0.4	0.068	0.385	17.8
0.5	0.085	0.44	20.2
0.6	0.102	0.49	22.2
0.7	0.119	0.53	23.7
0.8	0.136	0.565	24.9
0.9	0.153	0.60	26.0

Incoherent Scattering of Ag_2 Al : $I_i \cdot R(\frac{eu}{atom})$

$\frac{\sin\theta}{\lambda}$	0.1	0.15	0.2	0.3	0.4	0.5	0.6	0.7	0.8	0.9
I_i(Al)	1.2	2.4	3.5	5.2	6.3	7.3	8.1	8.7	9.1	9.4
I_i(Ag)	6.6	8.9	11.5	14.9	17.8	20.2	22.2	23.7	24.9	26.0
$I_i(Ag_2Al)\frac{1}{3}$	4.8	6.7	8.8	11.7	14.0	15.9	17.5	18.7	19.7	20.5

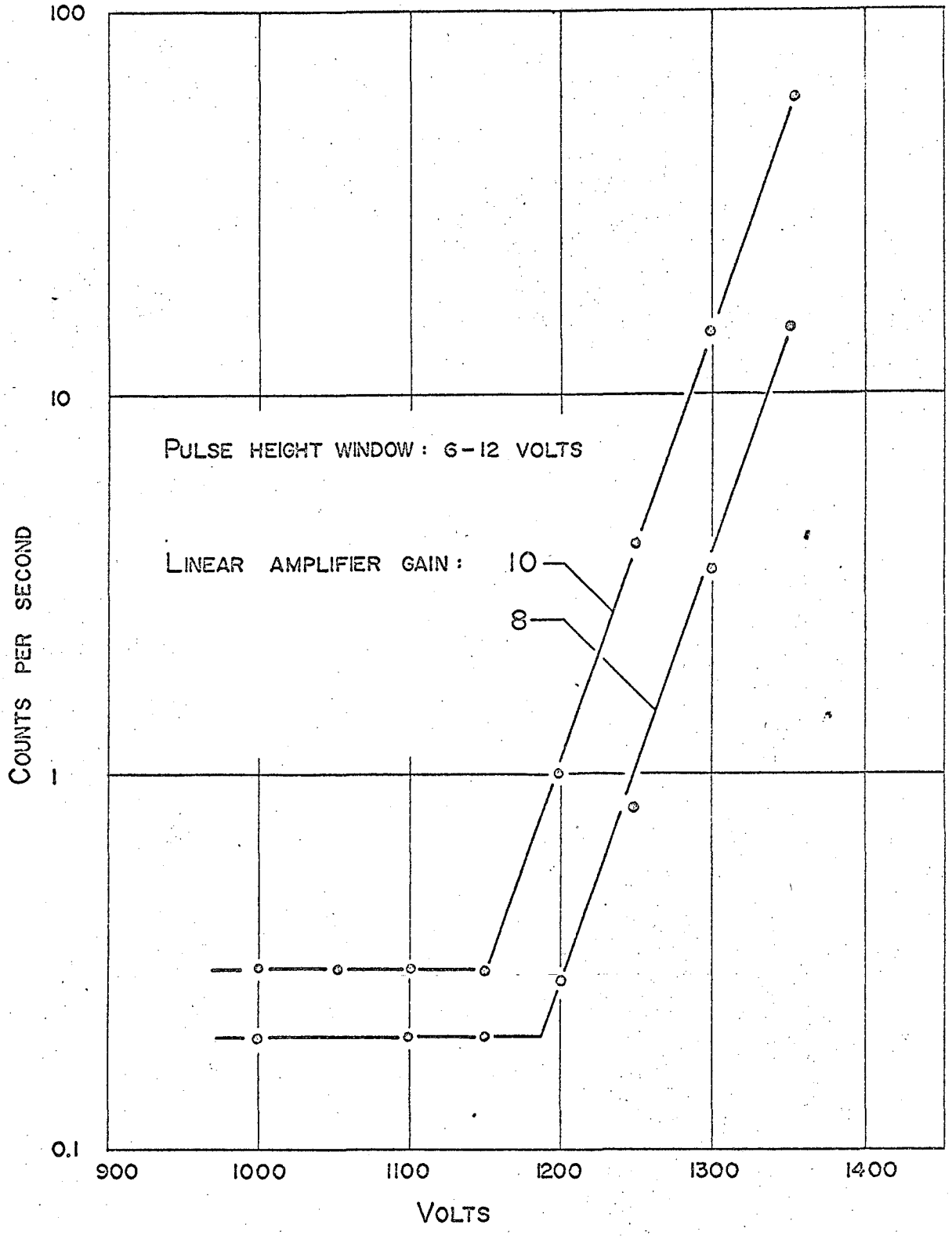

Fig. 4. NOISE LEVEL OF SCINTILLATION COUNTER AS A FUNCTION OF PHOTOMULTIPLIER VOLTAGE

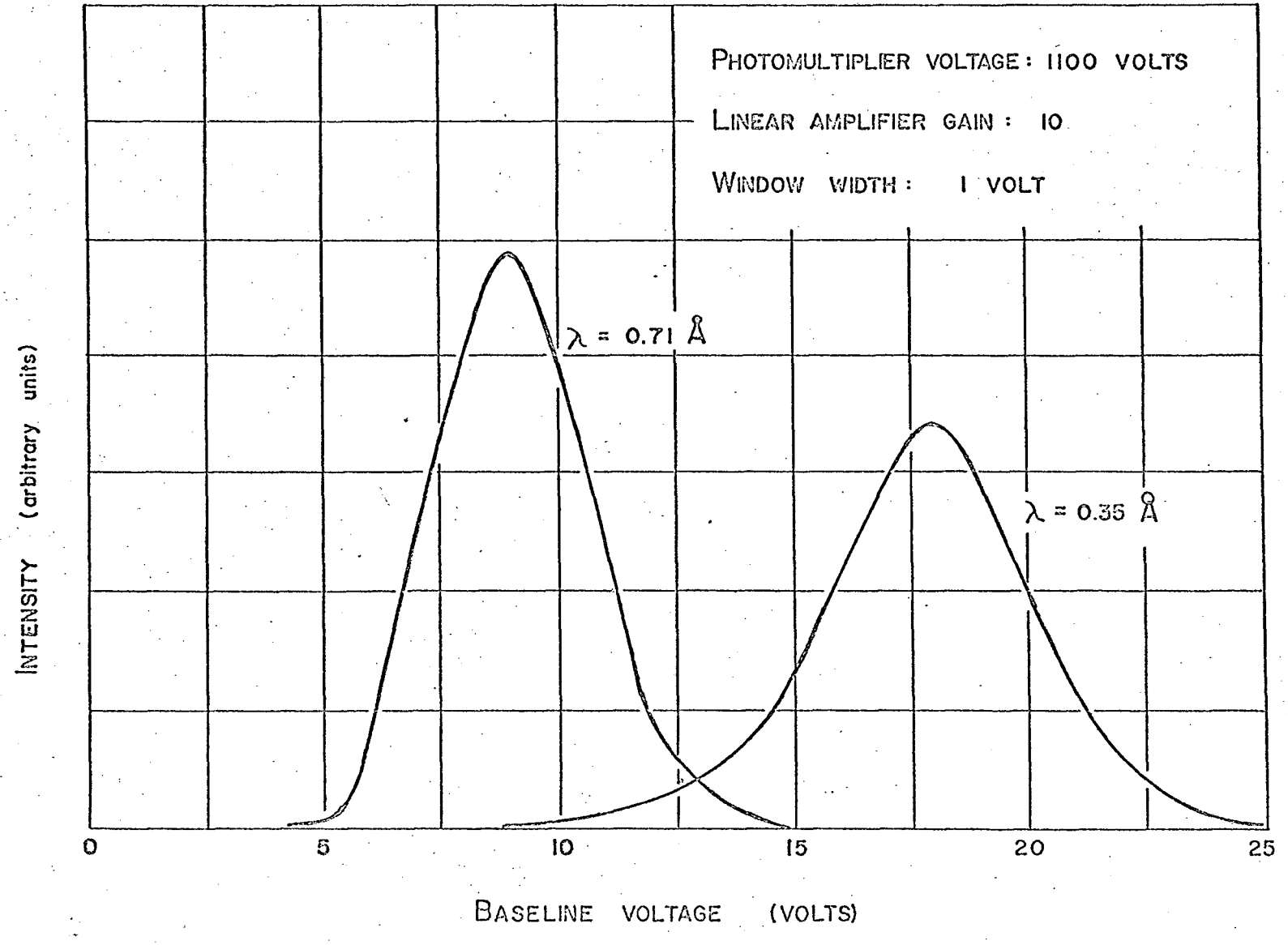

Fig. 5. PULSE-HEIGHT DISTRIBUTION OF $Mo - K_\alpha$ RADIATION AND ITS SECOND HARMONIC

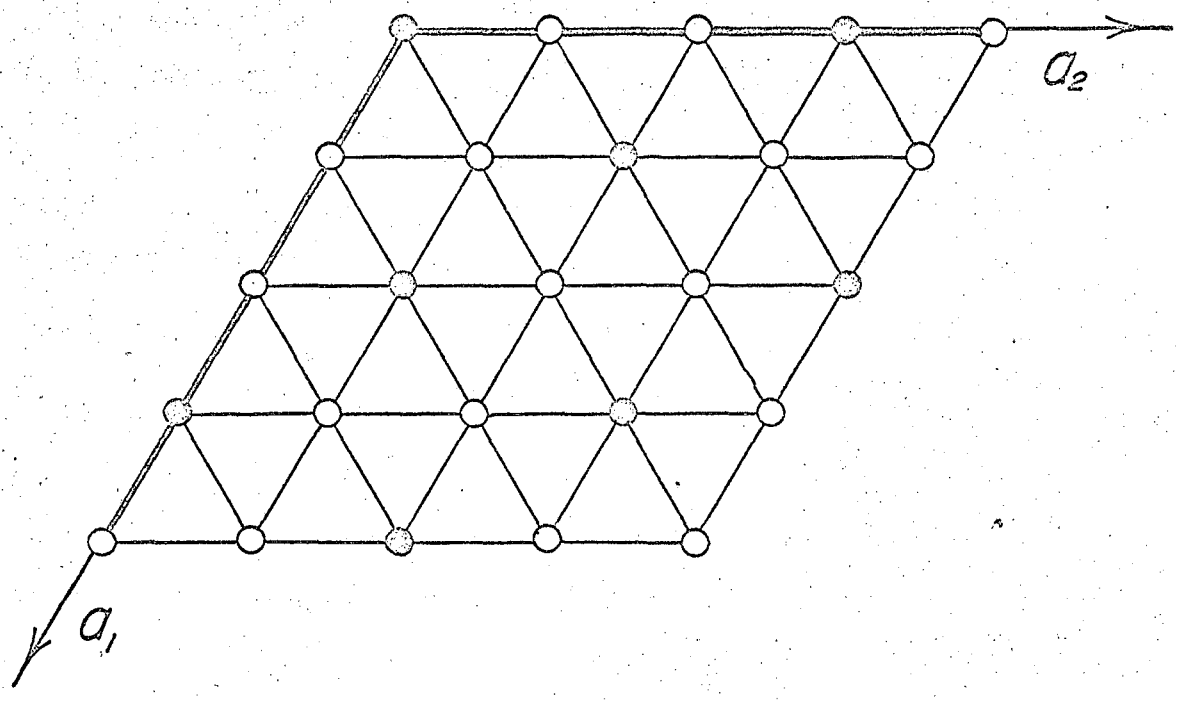

○ ALUMINUM

○ SILVER

Fig. 8. MODEL OF SUPER LATTICE IN BASAL PLANES

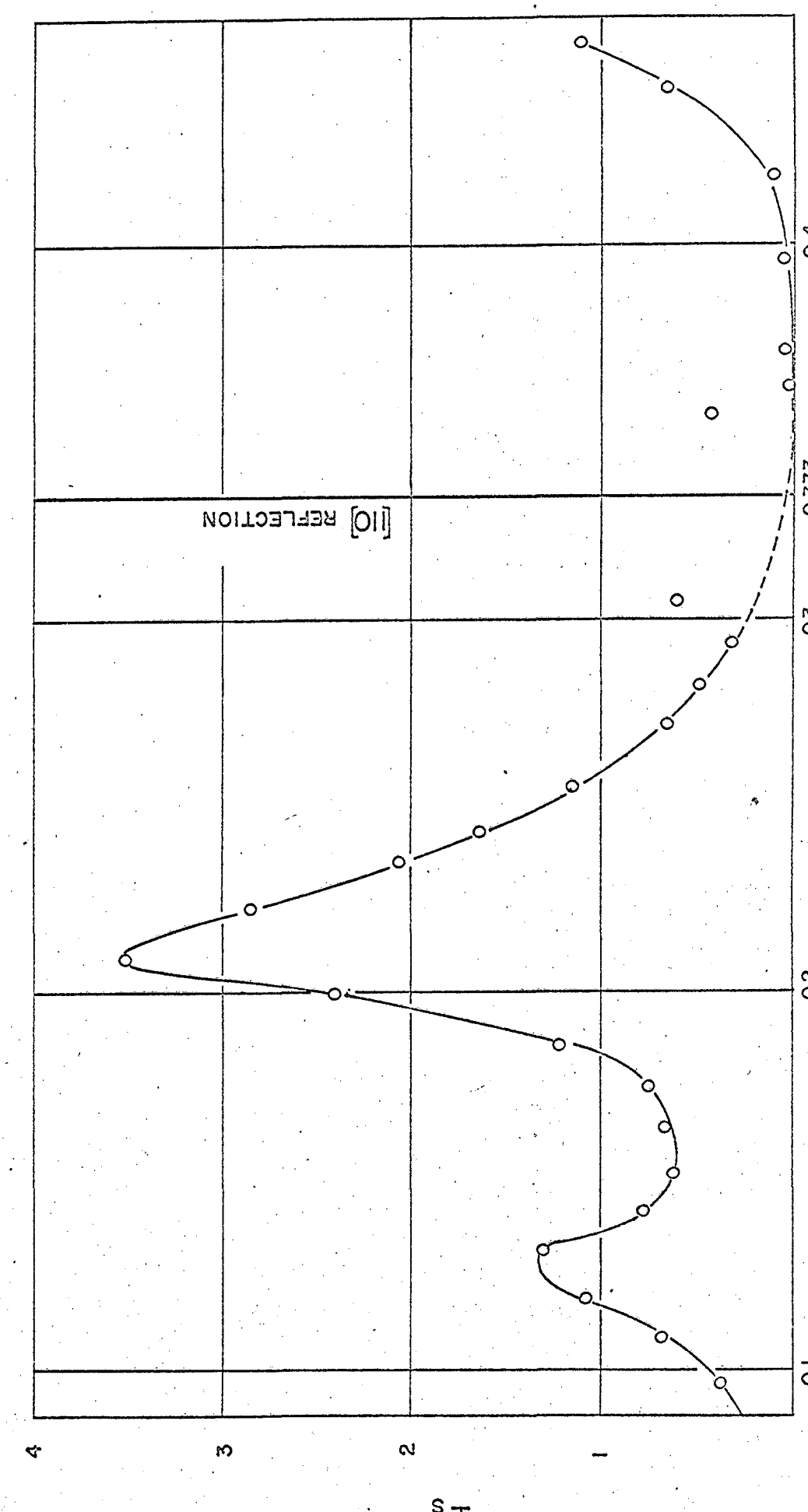

Fig. 9. LAUE-DIFFUSE INTENSITY ALONG [110]*